Mineralogical Magazine, June 2017, Vol. 81(3), pp. 723–736

Maneckiite, ideally $NaCa_2Fe^{2+}_2(Fe^{3+}Mg)Mn_2(PO_4)_6(H_2O)_2$, a new phosphate mineral of the wicksite supergroup from the Michałkowa pegmatite, Góry Sowie Block, southwestern Poland

Adam Pieczka[1,*], Frank C. Hawthorne[2], Bożena Gołębiowska[1], Adam Włodek[1] and Anna Grochowina[1]

[1] AGH University of Science and Technology, Department of Mineralogy, Petrography and Geochemistry 30-059 Kraków, Mickiewicza 30, Poland

[2] Department of Geological Sciences, University of Manitoba, Winnipeg, Manitoba R3T 2N2, Canada

[*Received 13 March 2016; Accepted 25 May 2016; Associate Editor: Anthony Kampf*]

ABSTRACT

Maneckiite, ideally $NaCa_2Fe^{2+}_2(Fe^{3+}Mg)Mn_2(PO_4)_6(H_2O)_2$, was found in a pegmatite at Michałkowa, Góry Sowie Block, SW Poland. The mineral forms subhedral and anhedral crystals ~150 μm × 150 μm in the outer zone of phosphate nodules, where it is associated with fluorapatite, wolfeite, Ca-rich graftonite and alluaudite-group minerals. Maneckiite is transparent, dark brown, with a colourless streak and vitreous lustre, brittle, and has a good cleavage //{010}, a splintery fracture and a Mohs hardness of ~5. The calculated density is 3.531 g cm^{-3}. Maneckiite is pleochroic: α = dark green, β = dark blue/green, γ = light brown/tan, biaxial (+) with refractive indices α = 1.698(2), β = 1.706(2), γ = 1.727(2) and birefringence Δ = ~0.03; $2V_{meas.}$ = 65.9 (1.5)° and $2V_{calc.}$ = 64°, dispersion is obscured by the dark colour, and optical orientation X//**a**, Y//**b**, Z//**c**. Maneckite is orthorhombic (*Pcab*) and has unit-cell parameters *a* = 12.526(4) Å, *b* = 12.914(5) Å, *c* = 11.664(4) Å and *V* = 1886.8(5) Å^3. The strongest reflections are (d_{hkl} in Å; *I*; *hkl*): 2.759, 100, 402; 2.916, 78, 004; 3.020, 68, 401; 2.844, 35, 014; 2.869, 31, 240; 2.825, 30, 042. Maneckiite has the wicksite structure and is its $^{M(3)}$Mn-analogue. The mineral crystallized as a product of Na- and Ca-metasomatism induced by a HT fluid in the presence of Al^{3+} from a neighbouring aluminosilicate melt. A Gladstone-Dale index, 0.027, places maneckiite in the category 'excellent'.

Keywords: maneckiite, wicksite supergroup, wicksite group, new mineral species, optical data, electron microprobe, crystal structure, LCT pegmatite, Michałkowa, Sudetes, Poland.

Introduction

The wicksite supergroup comprises four very rare and complex phosphate minerals: wicksite, bederite, tassieite and maneckiite, all forming the wicksite group of minerals, and one isostructural arsenate mineral, grischunite. Wicksite, $NaCa_2{}^{M(1)}Fe^{2+}_2{}^{M(2)}(Fe^{3+}Mg)^{M(3)}Fe^{2+}_2(PO_4)_6(H_2O)_2$, was found for the first time in the north-eastern Yukon Territory, Canada (Sturman *et al.*, 1981); bederite, $\square Ca_2{}^{M(1)}Mn^{2+M(2)}_2Fe^{3+M(3)}_2Mn^{2+}_2(PO_4)_6(H_2O)_2$, is only known from the El Peñón granitic pegmatite, Salta Province, República Argentina (Galliski *et al.*, 1999) and the Angarf-Sud pegmatite, Morocco (Kampf *et al.*, 2012); tassieite, $NaCa_2{}^{M(1)}Mg_2{}^{M(2)}(Fe^{3+}Mg)^{M(3)}Fe^{2+}_2(PO_4)_6(H_2O)_2$, from a secondary phosphate nodule collected between Johnston Fjord and Tassie Tarn, Stornes Peninsula, Larsemann Hills, Antarctica (Grew *et al.*, 2007); and maneckiite, $NaCa_2{}^{M(1)}Fe^{2+}_2{}^{M(2)}(Fe^{3+}Mg)^{M(3)}Mn_2(PO_4)_6(H_2O)_2$, was discovered in an anatectic pegmatite at Michałkowa, the Góry Sowie Block, Lower Silesia, SW Poland. The mineral has

*E-mail: pieczka@agh.edu.pl

https://doi.org/10.1180/minmag.2016.080.127

been approved by the International Mineralogical Association Commission on New Minerals, Nomenclature and Classification (IMA-CNMNC) (Pieczka *et al.*, 2015*a*; proposal 2015-056). Grischunite, $NaCa_2{}^{M(1)}Mn_2{}^{M(2)}(Fe^{3+}Mn)^{M(3)}Mn_2(AsO_4)_6(H_2O)_2$, is known only from the Falotta mine, Oberhalbstein, Graubunden Canton, Switzerland (Graeser *et al.*, 1984; Bianchi *et al.*, 1987), where it occurs as an alteration product of sarkinite, $Mn_2AsO_4(OH)$, in a former Mn deposit.

In this paper we describe maneckiite (pronunciation: 'manɛtskiit' in IPA for Polish), a new mineral of the wicksite group, as an ordered $^{M(3)}$Mn-analogue of wicksite. Maneckiite was found in a primitive, weakly fractionated anatectic pegmatite at Michałkowa, the Góry Sowie Block, Lower Silesia, SW Poland. The mineral is named in honour of Andrzej Manecki, an emeritus Professor at the Department of Mineralogy, Petrography and Geochemistry in the Faculty of Geology, Geophysics and Environmental Protection, AGH University of Science and Technology in Cracow, Poland, and one of the most eminent Polish mineralogists. Professor A. Manecki is one of the founders of the Mineralogical Society of Poland and, from 1988 to date, is the representative of the Mineralogical Society of Poland in the IMA-CNMNC.

The maneckiite holotype (specimen M4) and cotype (specimen M17) are deposited in the collection of the Mineralogical Museum of the University of Wrocław, Faculty of Earth Sciences and Environmental Management, Institute of Geological Sciences, 50-205 Wrocław, Cybulskiego 30, Poland, with catalogue numbers MMWr IV7674 and MMWr IV7677, respectively.

Geological setting

Maneckiite was collected at Michałkowa (50°45′N, 16°27′E), southeast of the Bystrzyckie Lake in the NW part of the Góry Sowie Block, ~70 km southwest of Wrocław, SW Poland (Fig. 1). The Góry Sowie Block is one of the main tectono-stratigraphic units (~650 km^2) of the Sudetes, the region that forms the NE margin of the Bohemian Massif and the NE termination of the European Variscides. The Góry Sowie Block unit consists mainly of gneisses and migmatites with minor amphibolites, and is considered to be a fragment of the lower crust (for details see Mazur *et al.*, 2006). The unit is a product of multistage evolution that culminated ~385–370 Ma in amphibolite-facies metamorphism and migmatization at temperatures of 775–910°C and pressures of 6.5–8.5 kb, and was followed by rapid uplift and exhumation (Brueckner *et al.*, 1996; O'Brien *et al.*, 1997; Kryza and Fanning, 2007). Anatectic melts generated by partial melting of the metasedimentary–metavolcanic sequence were injected as pegmatites and granite-like bodies during decompression stages, forming small concordant segregations and N-trending discordant dykes in migmatized gneisses and amphibolites (Kryza, 1981; van Breemen *et al.*, 1988; Żelaźniewicz, 1990; Bröcker *et al.*, 1998; Timmermann *et al.*, 2000; Aftalion and Bowes, 2002; Gordon *et al.*, 2005).

Maneckiite was collected on a small dump, a relic of excavation in the 19th century of central parts of the pegmatite as a source of raw quartz and feldspars. The dump is located on the left side of the Dział Michałowski Range, on the right side of the Młynówka stream, ~100 m from the road Zagórze Śląskie–Lubachów–Michałkowa–Pieszyce. Websky (1868) found the pegmatite and described a new phosphate mineral sarcopside (type locality), associated with hureaulite, vivianite and an apatite-group mineral. The original pegmatite, hosted by migmatitic gneiss and amphibolite, with usually sharp and well-defined contacts (*fide* Łodziński and Sitarz, 2009; Jabłońska, 2015), formed a vein ~10 m long and up to 2.5 m thick, with visible zoning [aplitic to medium-grained border zone (Qtz + Pl + Bt) – coarse-grained graphic zone (Qtz + Pl + Kfs + Bt + Msc) – blocky feldspar zone (Kfs + Pl > Qtz + Bt/Msc) – locally developed quartz core]. It is composed of plagioclase and microcline with P_2O_5 contents reaching 0.93 and 1.12 wt.%, respectively (Jabłońska, 2015), quartz, muscovite, biotite, foitite evolving to schorl, almandine, sillimanite, andalusite, base-metal sulphides (pyrrhotite, pyrite, chalcopyrite and sphalerite), extraordinarily rare beryl and columbite-(Fe) (Łodziński, 2007; Szełęg, pers. comm.), and phosphate minerals in nodules reaching a few centimetres in diameter.

Maneckiite was found in the outer zones of some small phosphate nodules, ~2 cm in diameter, composed mainly of lamellar intergrowths of primary magmatic phosphates sarcopside and graftonite, with minor triphylite oxidized topotactically to ferrisicklerite and heterosite. In the outer zone, the magmatic phosphates underwent intensive Na metasomatism and were replaced by wolfeite, hagendorfite and alluaudite-group minerals and fluorapatite, forming in places fine-grained mosaics. Lazulite, phosphosiderite, members of the phosphoferrite–kryzhanovskite series, jahnsite-group minerals, whitlockite and ferromerrillite, ferrostrunzite,

https://doi.org/10.1180/minmag.2016.080.127 Published online by Cambridge University Press

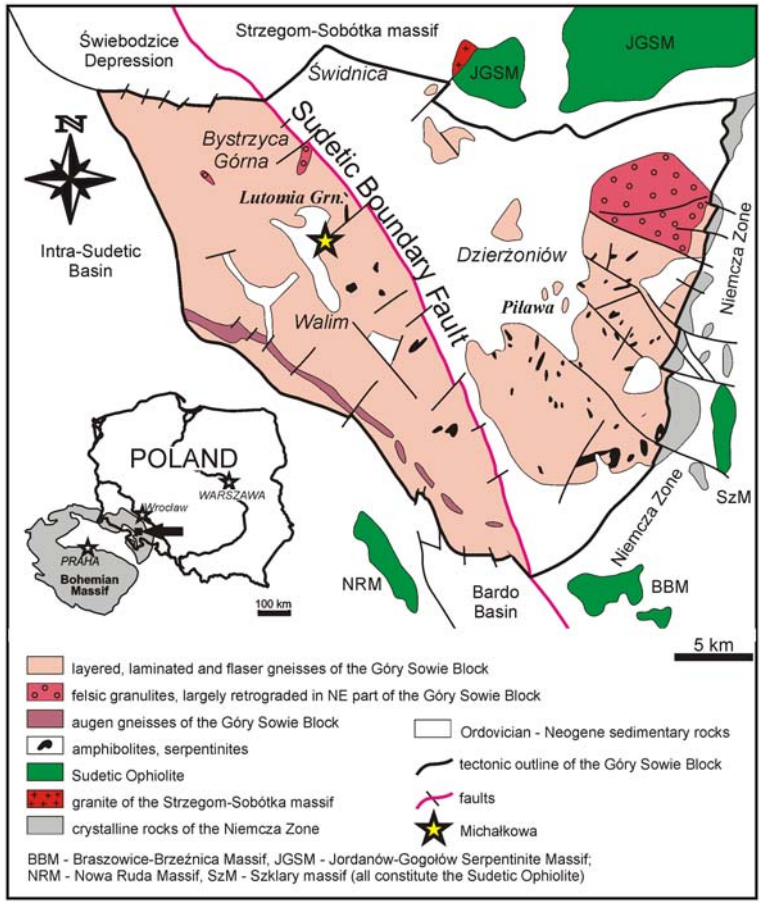

FIG. 1. Geological map of the Góry Sowie Block (after Szuszkiewicz *et al.*, 2013).

ludlamite, beraunite, arrojadite-group minerals and mitridatite are present in the nodules (Pieczka *et al.*, 2015*b*). Łodziński and Sitarz (2009) also reported willieite, ferrowyllieite, qingheiite, rosemaryite and simferite, but the presence of these phosphates in the pegmatite have not been confirmed either by chemical analysis or X-ray diffraction. The mineral composition allows classification of the pegmatite as a representative of the beryl–columbite–phosphate subtype of the REL–Li subclass of rare-element pegmatites *sensu* Černý and Ercit (2005) or the phosphate subtype of the rare-element class *sensu* Novák (2005).

Analytical methods

Electron-microprobe analyses of maneckiite were carried out at the Inter-Institute Analytical Complex for Minerals and Synthetic Substances of the University of Warsaw using a CAMECA SX 100 electron microprobe, operating in wavelength-dispersive spectroscopy (WDS) mode with an accelerating voltage of 15 kV, beam current of 20 nA, peak count-time of 20 s, background time of 10 s and a beam diameter of 2–5 μm. Standards, analytical lines, diffracting crystals and mean detection limits (wt.%) were as follows: albite – Na ($K\alpha$, TAP, 0.02), orthoclase – Al ($K\alpha$, TAP, 0.02), diopside – Mg ($K\alpha$, TAP, 0.02) and Ca ($K\alpha$, PET, 0.04), fluorapatite – P ($K\alpha$, PET, 0.03), rhodonite – Mn ($K\alpha$, LIF, 0.06), hematite – Fe ($K\alpha$, LIF, 0.06) and celestine – Sr ($L\alpha$, LPET, 0.07). The raw data were reduced with the *PAP* routine of Pouchou and Pichoir (1985). The empirical formulae of maneckiite were calculated first on the basis of 6 PO_4^{3-} anions per formula unit, using the measured P_2O_5 amounts [$P_2O_{5(meas.)}$]. However, results of such a calculation, i.e. totals of 2-valent

https://doi.org/10.1180/minmag.2016.080.127 Published online by Cambridge University Press

and 3-valent cations, varying in the range of 7.80–8.16 atoms per formula unit (apfu), and their mean content, 7.98 apfu, very close to the stoichiometric amount of 8 apfu, suggested: (1) complete occupancy of the octahedrally coordinated *M*(1)–*M*(3) and *Ca* sites; and (2) compositional effects caused by small inaccuracies in the microprobe P_2O_5 determination. It is obvious that such inaccuracies on the order 1–2% relative, i.e. 0.4–0.8 wt.% P_2O_5, result in inaccuracies of PO_4^{3-} determination in the range of 0.06–0.12 anions pfu, and possible variations in content of bivalent cations on the order 0.15–0.30 pfu and significant error in Fe^{3+}. Therefore, finally, all empirical formulae were normalized in relation to the total $Fe^{3+} + Fe^{2+} + Mn + Ca + Mg + Sr = 8$ apfu, with ideal contents of P_2O_5 calculated by stoichiometry [$P_2O_{5(calc.)}$]. Using this approach, the quality of the microprobe determination of P_2O_5 may be expressed through differences [$P_2O_{5(diff.)}$] between the WDS measured and calculated P_2O_5 amounts. The procedure is similar to the approach of Cámara *et al.* (2006) recommended for the calculation of formulae of the arrojadite-group minerals, i.e. another group of complex phosphates. The Fe_2O_3 and H_2O contents were obtained based on electroneutrality and the stoichiometry of the wicksite-group compounds. Results of the microprobe analysis of maneckiite in the holotype and co-type samples, along with calculated formulae for the mineral, are presented in Tables 1*a*, 1*b* and Table 2.

Single-crystal X-ray diffraction measurements were performed at the Department of Geological Sciences, University of Manitoba, Winnipeg, Canada, on a crystal (25 μm × 40 μm × 60 μm) attached to a tapered glass fibre and mounted on a Bruker APEX II ULTRA three-circle diffractometer equipped with a rotating-anode generator (Mo*K*α X-radiation), multilayer optics and an APEX-II 4 K CCD detector. A total of 68,217 intensities was collected to 60°2θ using 5 s per 0.2° frame-width with a crystal-to-detector distance of 5 cm. Empirical absorption corrections (*SADABS*; Sheldrick, 2008) were applied and equivalent reflections were merged, resulting in 2767 unique reflections, 2612 of which were above $|F_o| > 4\sigma|F|$. Unit-cell dimensions were obtained by least-squares refinement of the positions of 4012 reflections with $I > 10\sigma I$ and are given in Table 3, together with other information pertaining to data collection and structure refinement. Structure refinement, using *SHELXL-2014* (Sheldrick, 2015), was initiated with the atom coordinates of wicksite (Cooper and Hawthorne, 1997). Site-scattering values were considered as variable at the following sites and assigned scattering species: *M*(1) = Fe, *M*(2) = Fe, *M*(3) = Fe, *Ca* = Ca and *Na* = Na, and refinement progressed rapidly. At the final stages of refinement, it was apparent that the *M*(3) site was positionally disordered, and the site was split into three sub-sites with independent site-scattering values and isotropic-displacement parameters. Incident bond-valence indicated that O(13) is an (H_2O) group and the two strongest peaks in the difference-Fourier map were ~1 Å from O(13); these were inserted as H atoms into the refinement model with identical fixed displacement parameters and the O(13)–H distances constrained to be 0.98 Å. Refinement of all variables resulted in convergence at an R_1 index of 1.79%. Atom positions and equivalent isotropic-displacement parameters are given in Table 4, selected inter-atomic distances in Table 5, and refined site-scattering values (Hawthorne *et al.*, 1995) and assigned site-populations in Table 6. A powder X-ray diffraction pattern was not measured because of the compositional heterogeneity of the material. However, in Table 7 we provide a two-dimensional pattern by collapsing the three-dimensional diffraction data into two dimensions; using this technique, we can guarantee that the pattern is representative of the composition and crystal structure provided here.

Physical and optical properties

Maneckiite forms subhedral to anhedral, sometimes zoned, crystals ~150 μm × 150 μm in the outer zone of the phosphate nodules, where it is associated with fluorapatite, Ca-rich graftonite, alluaudite-group minerals and wolfeite (Fig. 2). Crystals of maneckiite usually occur close to the border of the metasomatic phosphates with the primary magmatic phosphates of the unaltered interior of the nodules, always close to fluorapatite.

Maneckiite is transparent, dark brown, with a colourless streak and vitreous lustre, and is non-fluorescent. The mineral is brittle with no observed partings, has a good cleavage //{010}, a splintery fracture and a Mohs hardness of ~5. Density was not measured due to the small crystals and common intergrowth with tiny grains of other phosphates (mainly wolfeite, alluaudite- and apatite-group minerals). The density calculated on the basis of the average molar weight and unit-cell volume for the refined crystal is equal to 3.531 g cm^{-3}.

Maneckiite is pleochroic (transmitted colour/relative absorption): α = dark green (maximum),

https://doi.org/10.1180/minmag.2016.080.127 Published online by Cambridge University Press

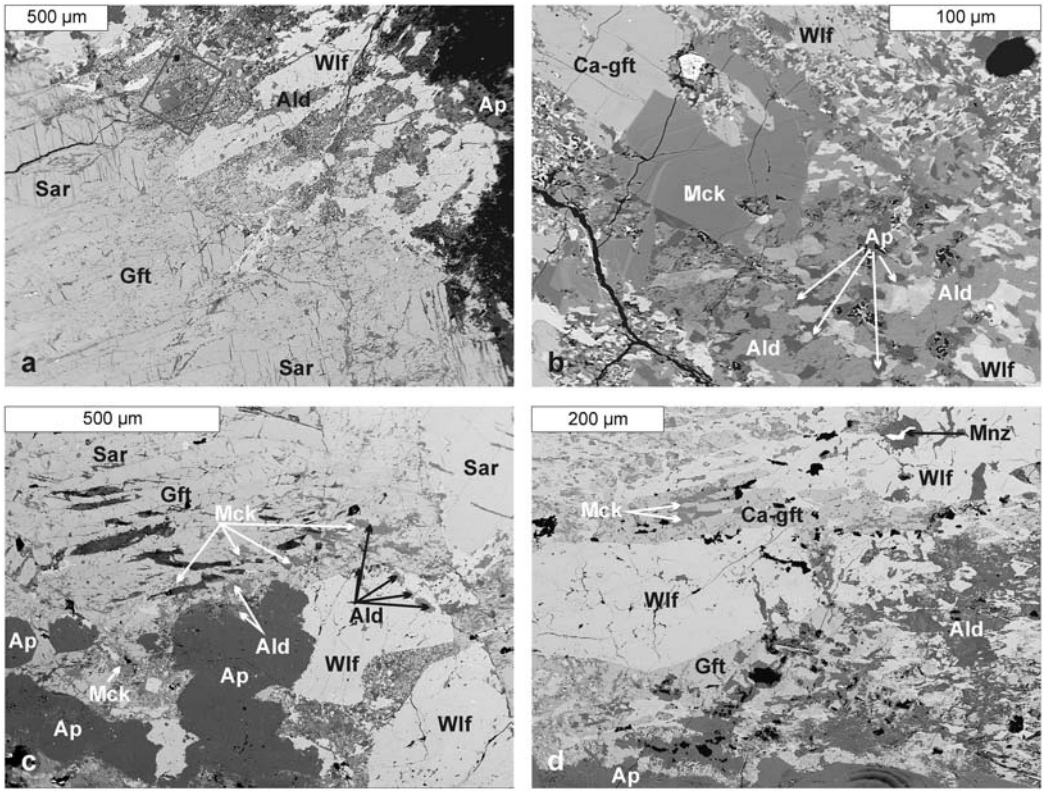

FIG. 2. (*a*) Fragment of the phosphate nodule with type maneckiite (in the area framed); (*b*) fragment of a zoned crystal of type maneckiite intergrown with Ca-bearing graftonite, partly replaced by a mosaic of metasomatic alluaudites, wolfeite and fluorapatite; and (*c*–*d*) maneckiite in the cotype sample. Abbreviations: Ald – an alluaudite-group mineral, Ap – fluorapatite, Ca-gft – Ca-rich graftonite, Gft – graftonite, Sar – sarcopside, Wlf – wolfeite, Mck – maneckiite, Mnz – monazite-(Ce).

β = dark blue/green (intermediate) and γ = light brown/tan (minimum), biaxial (+) with the following refractive indices: α = 1.698(2), β = 1.706(2) and γ = 1.727(2) and birefringence Δ = ~0.03. A spindle stage was used to orient a crystal for measurement of 2V by extinction curves (Bartelmehs *et al.*, 1992); $2V_{meas.}$ = 65.9 (1.5)° and $2V_{calc.}$ = 64° (589.9 nm). Dispersion is obscured by the dark colour of the crystal. The optical orientation, X//**a**, Y//**b**, Z//**c**, was determined by transferring the crystal from the spindle stage to a single-crystal diffractometer and measuring the relative axial relations by X-ray diffraction.

Composition

All the compositions collected in a compositionally zoned crystal of maneckiite in the holotype specimen (Fig. 2; Tables 1*a* and 1*b*) show almost complete occupancy of the *Na* site by Na, the *Ca* site by Ca and traces of Sr, and full occupancies of the octahedrally-coordinated *M*(1), *M*(2) and *M*(3) sites with various combinations of Fe^{2+}, Mn^{2+}, Mg^{2+} and Fe^{3+} cations. Assuming typical structural characteristics of the *M*(1) to *M*(3) sites in the earlier known members of the wicksite group (Cooper and Hawthorne, 1997; Galliski *et al.*, 1999; Grew *et al.*, 2007), it can be expected that the *M*(2) site should be filled dominantly by the smallest cations, i.e. Fe^{3+} and Mg^{2+}, whereas the *M*(3) site is filled dominantly by cations with the largest radii, i.e. Mn^{2+} or $Mn^{2+} + Fe^{2+}$. The *M*(1) site is commonly Fe^{2+} dominated, however, this site can also be partly filled with Mg^{2+}, as in tassieite (Grew *et al.*, 2007), or Mn^{2+}, as in bederite (Galliski *et al.*, 1999). Such assumptions lead to the following average formula of maneckiite in the holotype specimen: $(Na_{0.91}\square_{0.09})_{\Sigma=1.00}(Ca_{1.98}$

https://doi.org/10.1180/minmag.2016.080.127 Published online by Cambridge University Press

TABLE 1*a*. Electron-microprobe analyses of zoned maneckiite in the holotype specimen.

wt.%	1	2	3	4	5	6	7	8	9	10	11	12	13	14	Range	Mean	S.D.
$P_2O_{5(calc.)}$	42.92	42.98	41.62	41.92	42.32	41.94	41.82	42.78	43.15	43.68	42.30	42.37	41.50	41.80	41.50–43.68	42.36	0.65
$P_2O_{5(meas.)}$	42.99	43.46	41.62	42.41	42.00	42.09	42.05	42.37	43.37	43.21	42.60	42.10	41.47	42.10	40.93–43.81	42.45	0.78
$Fe_2O_{3(calc.)}$	8.81	9.88	8.64	8.75	8.18	7.82	8.04	9.14	9.13	9.58	8.85	8.55	7.93	7.87	7.82–9.87	8.65	0.64
$FeO_{(calc.)}$	14.43	13.86	17.48	15.27	16.44	16.66	16.53	13.64	14.65	12.70	14.26	14.49	17.17	14.99	12.70–17.48	15.19	1.45
MnO	9.70	11.24	12.04	11.10	11.46	12.06	12.12	10.94	8.82	10.75	11.60	12.29	14.57	14.32	8.82–14.57	11.64	1.53
CaO	11.10	11.23	10.99	10.99	11.06	11.11	11.06	10.78	11.06	11.13	11.17	11.00	11.02	11.28	10.78–11.28	11.07	0.12
MgO	6.21	5.33	2.61	4.53	4.23	3.63	3.50	6.02	6.72	6.78	4.94	4.73	1.59	3.03	1.59–6.78	4.56	1.58
SrO	0.68	b.d.l.	b.d.l.	b.d.l.	b.d.l.	b.d.l.	b.d.l.	0.36	0.45	0.58	b.d.l.	0.07	b.d.l.	b.d.l.	b.d.l.–0.68	0.15	0.25
Na_2O	2.83	2.42	2.71	2.73	2.98	3.07	2.97	2.68	2.74	2.64	2.72	2.85	2.96	3.03	2.42–3.07	2.81	0.18
$H_2O_{(calc.)}$	3.63	3.64	3.52	3.55	3.58	3.55	3.54	3.62	3.65	3.70	3.58	3.59	3.51	3.54	3.51–3.70	3.58	0.06
Total	100.31	100.58	99.60	98.81	100.27	99.84	99.58	99.95	100.35	101.54	99.42	99.93	100.26	99.84	98.81–101.54	100.02	0.63
$P_2O_{5(diff.)}$	0.07	0.48	0.00	0.52	–0.33	0.15	0.22	–0.40	0.22	–0.47	0.30	–0.28	–0.03	0.30	–0.47–0.52	0.05	0.32
$Fe^{3+} + Fe^{2+} + Mn + Ca + Mg + Sr = 8$ apfu and $P_{(calc.)}O_4^{3-} = 6$ pfu																	
PO_4^{3-}	6.00	6.00	6.00	6.00	6.00	6.00	6.00	6.00	6.00	6.00	6.00	6.00	6.00	6.00	6.00	6.00	
Fe^{3+}	1.10	1.23	1.11	1.10	1.03	0.99	1.02	1.14	1.13	1.17	1.12	1.08	1.02	1.00	0.99–1.23	1.09	0.07
Fe^{2+}	1.99	1.91	2.49	2.17	2.30	2.35	2.34	1.89	2.01	1.72	2.00	2.03	2.45	2.12	1.72–2.49	2.12	0.23
Mn^{2+}	1.36	1.57	1.74	1.59	1.63	1.73	1.74	1.54	1.23	1.48	1.65	1.74	2.11	2.06	1.23–2.11	1.65	0.24
Ca^{2+}	1.96	1.98	2.01	1.99	1.98	2.01	2.01	1.91	1.95	1.94	2.01	1.97	2.02	2.05	1.91–2.05	1.98	0.04
Mg^{2+}	1.53	1.31	0.66	1.14	1.06	0.91	0.88	1.49	1.64	1.64	1.23	1.18	0.41	0.76	0.41–1.64	1.14	0.38
Sr^{2+}	0.07	0.00	0.00	0.00	0.00	0.00	0.00	0.03	0.04	0.05	0.00	0.01	0.00	0.00	0.00–0.07	0.01	0.02
Na^+	0.90	0.77	0.89	0.90	0.97	1.01	0.98	0.86	0.87	0.83	0.88	0.92	0.98	1.00	0.77–1.01	0.91	0.07
H_2O	2	2	2	2	2	2	2	2	2	2	2	2	2	2	2	2	
#Mn	0.41	0.45	0.41	0.42	0.41	0.42	0.43	0.45	0.38	0.46	0.45	0.46	0.46	0.49	0.38–0.49	0.44	0.03

#Mn = Mn/(Mn + Fe); b.d.l. – below detection limit.
S.D. – standard deviation

TABLE 1*b*. *M*(1)–*M*(3) site occupancies and corresponding calculated mean bond lengths in the holotype maneckiite estimated on the basis of electron-microprobe analyses.*

	1	2	3	4	5	6	7	8	9	10	11	12	13	14	Range	Mean	S.D.
$^{M(1)}Fe^{2+}$	1.35	1.48	1.99	1.76	1.93	1.99	1.99	1.43	1.24	1.20	1.64	1.77	1.88	1.89	1.20–1.99	1.77	0.29
$^{M(1)}Mn^{2+}$	0.00	0.00	0.00	0.00	0.00	0.00	0.00	0.00	0.00	0.00	0.00	0.00	0.11	0.06	0.00–0.11	0.00	0.03
$^{M(1)}Mg^{2+}$	0.62	0.53	0.00	0.25	0.09	0.00	0.00	0.63	0.77	0.81	0.35	0.26	0.00	0.00	0.00–0.81	0.23	0.31
Σ*M*(1)	1.97	2.02	1.99	2.01	2.02	1.99	1.99	2.05	2.01	2.01	1.99	2.02	1.98	1.95	1.95–2.05	2.00	0.02
<*M*(1)–O> (Å)	2.12	2.12	2.14	2.13	2.14	2.14	2.14	2.12	2.12	2.12	2.13	2.13	2.14	2.14	2.11–2.14	2.13	0.01
$^{M(2)}Fe^{3+}$	1.10	1.23	1.11	1.10	1.03	0.99	1.02	1.13	1.13	1.17	1.12	1.08	1.02	1.00	0.99–1.23	1.09	0.07
$^{M(2)}Mg^{2+}$	0.90	0.77	0.66	0.90	0.97	0.91	0.88	0.87	0.87	0.83	0.88	0.92	0.41	0.76	0.41–0.97	0.91	0.14
$^{M(2)}Fe^{2+}$	0.00	0.00	0.23	0.00	0.00	0.09	0.09	0.00	0.00	0.00	0.00	0.00	0.57	0.23	0.00–0.57	0.00	0.16
Σ*M*(2)	2.00	2.00	2.00	2.00	2.00	2.00	2.00	2.00	2.00	2.00	2.00	2.00	2.00	2.00	2.00	2.00	
<*M*(2)–O> (Å)	2.04	2.03	2.05	2.04	2.04	2.05	2.04	2.04	2.04	2.04	2.04	2.04	2.06	2.05	2.03–2.06	2.04	0.01
$^{M(3)}Mn^{2+}$	1.36	1.57	1.74	1.59	1.63	1.73	1.74	1.54	1.23	1.48	1.65	1.74	2.00	2.00	1.23–2.00	1.65	0.21
$^{M(3)}Fe^{2+}$	0.64	0.43	0.26	0.41	0.37	0.27	0.26	0.46	0.77	0.52	0.35	0.26	0.00	0.00	0.00–0.77	0.35	0.21
Σ*M*(3)	2.00	2.00	2.00	2.00	2.00	2.00	2.00	2.00	2.00	2.00	2.00	2.00	2.00	2.00	2.00	2.00	
<*M*(3)–O> (Å)	2.17	2.18	2.18	2.18	2.18	2.18	2.18	2.18	2.17	2.18	2.18	2.18	2.19	2.19	2.17–2.19	2.18	0.01

*Mean bond lengths <*M*(1)–O>, <*M*(2)–O> and <*M*(3)–O> are calculated on the basis of Shannon's (1976) ionic radii (http://abulafia.mt.ic.ac.uk/shannon/). Note predomination of Fe^{2+} at the *M*(1) site, Fe^{3+} at the *M*(2) site and Mn^{2+} at the *M*(3) site, suggesting the composition $NaCa_2Fe^{2+}_2(Fe^{3+}Mg)Mn_2(PO_4)_6(H_2O)_2$ for the new mineral maneckiite.
S.D. – standard deviation

TABLE 2. Representative electron-microprobe analyses of maneckiite in the cotype specimen.*

wt.%	1	2	3	5	6	7	9	10
$P_2O_{5(calc.)}$	41.87	41.17	43.33	42.76	42.90	43.40	43.02	41.06
P_2O_5	41.48	41.59	42.85	42.94	43.17	43.34	42.44	41.71
Al_2O_3	b.d.l.	b.d.l.	0.93	b.d.l.	b.d.l.	2.98	0.56	0.54
$Fe_2O_{3(calc.)}$	9.04	8.11	8.06	8.54	9.00	4.74	8.48	6.80
$FeO_{(calc.)}$	15.14	18.01	12.38	13.61	14.27	21.02	18.52	18.06
MnO	13.88	13.00	11.79	12.20	11.55	7.59	10.04	13.08
CaO	10.80	11.18	11.33	11.39	11.13	11.13	11.26	10.91
MgO	3.00	1.56	6.22	5.31	5.37	4.00	3.66	1.83
Na_2O	2.59	2.84	2.62	2.91	2.75	2.66	2.63	3.01
$H_2O_{(calc.)}$	3.54	3.48	3.67	3.62	3.63	3.67	3.64	3.47
Total	99.87	99.36	100.31	100.34	100.61	101.20	101.81	98.76
$P_2O_{5(diff.)}$	−0.40	0.42	−0.48	0.18	0.26	−0.05	−0.57	0.65
	$Fe^{3+} + Fe^{2+} + Mn + Ca + Mg + Sr = 8$ apfu and $P_{(calc.)}O_4^{3-} = 6$ pfu							
Na^+	0.85	0.95	0.83	0.93	0.88	0.84	0.84	1.01
Ca^{2+}	1.96	2.06	1.99	2.02	1.97	1.95	1.99	2.02
$^{M(1)}Fe^{2+}$	2.04	1.94	1.33	1.60	1.59	1.92	1.95	1.98
$^{M(1)}Mn^{2+}$	0.00	0.00	0.00	0.00	0.00	0.00	0.00	0.00
$^{M(1)}Mg^{2+}$	0.00	0.00	0.69	0.38	0.44	0.13	0.06	0.00
Σ*M*(1)	2.04	1.94	2.01	1.98	2.03	2.05	2.01	1.98
<*M*(1)–O> (Å)	2.14	2.14	2.12	2.13	2.13	2.14	2.14	2.14
$^{M(2)}Fe^{3+}$	1.15	1.05	0.99	1.07	1.12	0.58	1.05	0.88
$^{M(2)}Al^{3+}$	0.00	0.00	0.18	0.00	0.00	0.57	0.11	0.11
$^{M(2)}Mg^{2+}$	0.76	0.40	0.83	0.93	0.88	0.84	0.84	0.47
$^{M(2)}Fe^{2+}$	0.09	0.55	0.00	0.00	0.00	0.00	0.00	0.54
Σ*M*(2)	2.00	2.00	2.00	2.00	2.00	2.00	2.00	2.00
<*M*(2)–O> (Å)	2.04	2.06	2.03	2.04	2.04	2.01	2.03	2.05
$^{M(3)}Mn^{2+}$	1.99	1.90	1.63	1.71	1.62	1.05	1.40	1.91
$^{M(3)}Fe^{2+}$	0.01	0.10	0.37	0.29	0.38	0.95	0.60	0.09
Σ*M*(3)	2.00	2.00	2.00	2.00	2.00	2.00	2.00	2.00
<*M*(3)–O> (Å)	2.19	2.19	2.18	2.18	2.18	2.17	2.18	2.19
PO_4^{3-}	6.00	6.00	6.00	6.00	6.00	6.00	6.00	6.00
H_2O	2	2	2	2	2	2	2	2
#Mn	0.48	0.42	0.49	0.48	0.45	0.27	0.35	0.42

*Mean bond lengths <*M*(1)–O>, <*M*(2)–O> and <*M*(3)–O> are calculated on the basis of Shannon's (1976) ionic radii (http://abulafia.mt.ic.ac.uk/shannon/). Note the presence of Al^{3+} substituting for Fe^{3+} in contrast to the holotype crystal. The Al content can be close to the Fe^{3+}, although no analysis with $Al^{3+} > Fe^{3+}$ has been found to date. Note also that increasing Al^{3+} relates to analyses with decreasing Mn, thus compositions with Al^{3+} present correspond to low Mn–Fe fractionation and probably early crystallization.

$Sr_{0.01})_{\Sigma=2.00}{}^{M(1)}(Fe^{2+}_{1.77}Mg_{0.23})_{\Sigma=2.00}{}^{M(2)}(Fe^{3+}_{1.09}Mg_{0.91})_{\Sigma=2.00}{}^{M(3)}(Mn_{1.65}Fe^{2+}_{0.35})_{\Sigma=2.00}(PO_4)_6(H_2O)_2$, with the calculated mean bond lengths <*M*(1)–O> = 2.13(1) Å, <*M*(2)–O> = 2.04(1) Å and <*M*(3)–O> = 2.18(1) Å and site-scattering values of 48.9, 39.2 and 50.3 electrons per formula unit (epfu) (Table 1*b*). Similar quantitative relations among the respective cations were found for some maneckiite crystals in the co-type specimen, representing another phosphate nodule (Table 2), with one important addition, viz. the presence of Al_2O_3 in varying amounts, reaching almost 3 wt.%. Alumina, Al_2O_3 has already been observed in members of the wicksite group, e.g. in bederite (Galliski *et al.*, 1999); however, the highest contents were much lower, reaching only 1.2 wt.%, and the

https://doi.org/10.1180/minmag.2016.080.127 Published online by Cambridge University Press

TABLE 3. Miscellaneous information for maneckiite.

a (Å)	12.526(4)	Crystal size (μm)	25 × 40 × 60
b	12.914(5)	Radiation	Mo*K*α
c	11.664(4)	No. of reflections	68,217
α (°)	90°	No. unique reflections	2767
β	90°	No. with ($F_o > 4\sigma F$)	2612
γ	90°	R_{int} %	2.62
V (Å^3)	1886.8(5)	R_1%	1.79
Space group	*Pcab*	wR_2%	5.17
Z	4		

Ideal cell content: 4 $NaCa_2Fe_2^{2+}(Fe^{3+}Mg)Mn_2(PO_4)_6(H_2O)_2$

$R_1 = \Sigma(|F_o| - |F_c|)/\Sigma|F_o|$

$wR_2 = [\Sigma w\ (F_o^2 - F_c^2)^2/\Sigma w\ (F_o^2)^2\ ]^{½}$, $w = 1/[\sigma^2(F_o^2) + (0.0160\ P)^2 + 4.09\ P]$, $P = (\mathrm{Max}(F_o^2,0) + 2F_c^2)/3$

substitution of Al^{3+} for Fe^{3+} at the *M*(2) site was less significant. In co-type maneckiite, the Al content, reaches 0.57 apfu, and is similar to Fe^{3+} for the same analytical spot (cf. analysis 7 in Table 2); however, Al is never greater than Fe^{3+}. This indicates that Fe^{3+} can be substituted extensively by Al^{3+} in phosphate minerals of the wicksite supergroup, at least up to $Al^{3+} \approx Fe^{3+}$. In consequence, a member of the wicksite supergroup with $Al \gg Fe^{3+}$ seems to be possible in Nature. From the above discussion, the simplified maneckiite formula may be written as $NaCa_2{}^{M(1)}Fe_2^{2+}{}^{M(2)}[(Fe^{3+},Al)Mg]^{M(3)}Mn_2(PO_4)_6(H_2O)_2$. Thus maneckiite is the $^{M(3)}$Mn analogue of wicksite. A Gladstone-Dale index (Mandarino, 1981) of the physical and chemical data for maneckiite = 0.027 places the mineral in the category 'excellent'.

Crystal structure

Maneckiite has the wicksite structure (cf. Cooper and Hawthorne, 1997), with the refined site-scattering values and assigned site-populations given in Table 6. The refined site-scattering values at the *Ca* and *Na* sites indicate that these sites are dominated by Ca^{2+} and Na^+, respectively, in accord with the observed mean bond lengths (Table 6). The total site-scattering at the *M*(1)–*M*(3) sites is in accord with occupancy by Mg, Fe and Mn as indicated by the chemical formulae (Table 1*b*). The individual site-scattering values may be used to derive the amounts of Mg and Mn-Fe at the *M*(1)–*M*(3) sites. The mean bond lengths indicate that Fe^{3+} must occur at the *M*(2) site, in accord with previous refinements of wicksite-group minerals. The large mean bond lengths for the *M*(3) and *M*(3A) sites indicate that the (Mn-Fe) assigned to these sites must be dominated by Mn^{2+} and the intermediate mean bond length for *M*(1) indicate that the (Mn-Fe) assigned to this site must be dominated by Fe^{2+}. The sum of the constituent ionic radii (Table 6) are in reasonable accord with the observed mean bond lengths at the *M*(1) and *M*(2) sites. Minor Mn^{2+} could occur at *M*(1) and minor Fe^{2+} could occur at *M*(3), but the site preferences *M*(3) > *M*(1) for Mn^{2+} and *M*(1) > *M*(3) for Fe^{2+} are well-established. The <*M*(1)–O> and <*M*(2)–O> distances, 2.134 Å and 2.046 Å, respectively, and the mean bond lengths of 2.200, 2.171 and 2.112 Å for the three *M*(3) sub-sites (Table 5) correspond closely to the values suggested in Table 1*b*. In consequence, the resultant composition of the refined crystal lies well within the range of compositions found in the holotype specimen (Table 1*b*). Based on the site populations assigned in Table 7, the dominant end-member composition formula of maneckiite may be written as $NaCa_2Fe_2^{2+}(Fe^{3+}Mg)Mn_2(PO_4)_6(H_2O)_2$. There is minor vacancy at the *Na* site that is compensated by excess Fe^{3+} at the *M*(2) site, and extensive disorder of the *M*(3) cations that give rise to various different short-range arrangements in this part of the structure.

Relation to other species

Maneckite is the fourth member of the wicksite group within the wicksite supergroup, beside wicksite (Sturman *et al.*, 1981), bederite (Galliski *et al.*, 1999) and tassieite (Grew *et al.*, 2007), and due to Mn^{2+} ordering at the *M*(3) site, it can be considered as the $^{M(3)}$Mn-analogue of wicksite. It has Fe^{2+} completely ordered at the *M*(1) site, Fe^{3+} = Mg at the *M*(2)

https://doi.org/10.1180/minmag.2016.080.127 Published online by Cambridge University Press

TABLE 4. Atom coordinates and displacement parameters for maneckiite.

Atom	*x*	*y*	*z*	U^{11}	U^{22}	U^{33}	U^{23}	U^{13}	U^{12}	U_{eq}
P(1)	0.39091(3)	0.30157(3)	0.22559(3)	0.00737(16)	0.00716(17)	0.00715(17)	–0.00057(12)	–0.00012(13)	0.00009(12)	0.00723(9)
P(2)	0.10079(3)	0.44369(3)	0.25421(3)	0.00697(16)	0.00721(16)	0.00772(16)	0.00006(13)	–0.00024(12)	–0.00018(12)	0.00730(9)
P(3)	0.26728(3)	0.12477(3)	0.47608(4)	0.00988(17)	0.00702(17)	0.00731(17)	–0.00023(12)	–0.00025(12)	–0.00004(11)	0.00807(9)
M(1)	0.15370(2)	0.20718(2)	0.22753(3)	0.00949(14)	0.00926(14)	0.01191(15)	0.00129(9)	0.00090(9)	0.00048(9)	0.01022(9)
M(2)	0.33315(2)	0.04319(2)	0.22589(2)	0.00787(14)	0.00787(14)	0.00799(14)	–0.00036(9)	–0.00002(9)	0.00023(8)	0.00791(9)
M(3)	0.0322(3)	0.26437(18)	0.45456(9)							0.0103(3)
M(3)1	0.0156(3)	0.2745(2)	0.45738(3)							0.0082(4)
M(3)2	–0.0053(6)	0.3059(9)	0.4596(4)							0.0135(17)
Ca	0.26359(3)	0.37467(2)	0.49465(3)	0.01134(16)	0.01103(16)	0.01020(16)	0.00155(10)	–0.00095(10)	–0.00163(9)	0.01086(10)
Na	0	0	0	0.0252(7)	0.0374(9)	0.0426(10)	0.0259(7)	–0.0093(6)	0.0055(6)	0.0357(5)
O(1)	0.49847(9)	0.27490(9)	0.28223(10)	0.0089(5)	0.0144(5)	0.0118(5)	–0.0009(4)	–0.0022(4)	0.0021(4)	0.0117(2)
O(2)	0.40840(9)	0.33886(9)	0.10180(9)	0.0145(5)	0.0134(5)	0.0081(5)	0.0011(4)	0.0010(4)	0.0011(4)	0.0120(2)
O(3)	0.32116(9)	0.20318(8)	0.22145(10)	0.0106(5)	0.0090(5)	0.0166(5)	–0.0008(4)	0.0001(4)	–0.0019(4)	0.0121(2)
O(4)	0.33555(9)	0.38507(8)	0.29858(10)	0.0095(5)	0.0107(5)	0.0107(5)	–0.0025(4)	0.0005(4)	0.0009(4)	0.0103(2)
O(5)	0.16610(9)	0.54494(8)	0.25545(10)	0.0122(5)	0.0090(5)	0.0128(5)	0.0002(4)	–0.0003(4)	–0.0022(4)	0.0113(2)
O(6)	0.15482(9)	0.36292(9)	0.17790(10)	0.0110(5)	0.0098(5)	0.0119(5)	–0.0020(4)	0.0006(4)	0.0009(4)	0.0109(2)
O(7)	0.09318(9)	0.40455(9)	0.37896(10)	0.0146(5)	0.0123(5)	0.0086(5)	0.0014(4)	–0.0004(4)	–0.0019(4)	0.0118(2)
O(8)	–0.00984(9)	0.46649(90)	0.20187(11)	0.0094(5)	0.0156(6)	0.0152(6)	0.0002(4)	–0.0023(4)	0.0028(4)	0.0134(2)
O(9)	0.19234(9)	0.20396(8)	0.41698(10)	0.0131(5)	0.0102(5)	0.0119(5)	0.0013(4)	0.0002(4)	0.0028(4)	0.0117(2)
O(10)	0.35217(9)	0.19020(9)	0.54085(10)	0.0151(5)	0.0149(5)	0.0121(5)	–0.0020(4)	–0.0016(4)	–0.0053(4)	0.0141(2)
O(11)	0.20087(9)	0.05233(8)	0.55362(10)	0.0161(5)	0.0098(5)	0.0106(5)	0.0018(4)	–0.0010(4)	–0.0027(4)	0.0121(2)
O(12)	0.33007(10)	0.05206(9)	0.39610(10)	0.0176(6)	0.0154(6)	0.0112(5)	–0.0029(4)	–0.0016(4)	0.0079(4)	0.0147(3)
O(13)	–0.02769(10)	0.11643(9)	0.48697(10)	0.0167(6)	0.0165(6)	0.0122(5)	0.0027(4)	0.0001(4)	0.0016(4)	0.0151(2)
H(1)	–0.0004(17)	0.0890(17)	0.5596(10)							0.02*
H(2)	–0.0070(18)	0.0759(15)	0.4195(12)							0.02*

*Fixed during the refinement.

TABLE 5. Selected interatomic distances (Å) in maneckiite.

P(1)–O(1)	1.540(1)	*Ca*–O(2)e	2.533(1)	*M*(1)–O(1)a	2.060(1)	*M*(3)–O(1)a	2.116(1)
P(1)–O(2)	1.538(1)	*Ca*–O(4)	2.462(1)	*M*(1)–O(3)	2.099(1)	*M*(3)–O(2)e	2.104(1)
P(1)–O(3)	1.543(1)	*Ca*–O(6)e	2.374(1)	*M*(1)–O(5)b	2.110(1)	*M*(3)–O(7)	2.154(1)
P(1)–O(4)	1.539(1)	*Ca*–O(7)	2.555(1)	*M*(1)–O(6)	2.093(1)	*M*(3)–O(9)	2.196(1)
<*P*(1)–O>	1.540	*Ca*–O(9)	2.545(1)	*M*(1)–O(9)	2.263(1)	*M*(3)–O(10)a	2.538(1)
		Ca–O(11)f	2.404(1)	*M*(1)–O(10)c	2.190(1)	*M*(3)–O(13)	2.087(1)
P(2)–O(5)	1.542(1)	*Ca*–O(13)d	2.619(1)	<*M*(1)–O>	2.134	<*M*(3)–O>	2.200
P(2)–O(6)	1.529(1)	*Ca*–O(10)	2.683(1)				
P(2)–O(7)	1.543(1)	<*Ca*–O>	2.522	*M*(2)–O(3)	2.072(1)	*M*(3)1–O(1)a	2.151(2)
P(2)–O(8)	1.543(1)			*M*(2)–O(4)b	2.062(1)	*M*(3)1–O(2)e	2.106(2)
<*P*(2)–O>	1.539	*Na*–O(7)b,g	2.208(1)	*M*(2)–O(5)b	2.104(1)	*M*(3)1–O(7)	2.145(1)
		Na–O(12)c,h	2.540(1)	*M*(2)–O(8)d	1.991(1)	*M*(3)1–O(10)a	2.313(2)
P(3)–O(9)	1.550(1)	*Na*–O(2)a,i	2.656(1)	*M*(2)–O(11)c	2.057(1)	*M*(3)1–O(13)	2.140(2)
P(3)–O(10)	1.554(1)	<*Na*–O>	2.468	*M*(2)–O(12)	1.989(1)	<*M*(3A)–O>	2.171
P(3)–O(11)	1.545(1)			<*M*(2)–O>	2.046		
P(3)–O(12)	1.540(1)					*M*(3)2–O(1)a	2.317(7)
<*P*(3)–O>	1.547			*M*(3)–*M*(3B)	0.72(1)	*M*(3)2–O(2)e	2.099(5)
						M(3)2–O(7)	2.007(6)
						M(3)2–O(10)a	2.022(7)
						<*M*(3)2–O>	2.112

Symmetry codes: a: x–1/2,½–y,z; b: x,y–1/2,1/2–z; c: ½–x,y,z–1/2; d: x + 1/2,1/2–y,z; e: ½–x,y,z + 1/2; f: ½–x,y + 1/2,1–z; g: –x,1/2–y,z–1/2; h: x–1/2,–y,1/2–z; i: 1/2–x,y–1/2,–z.

site, and Mn^{2+} completely ordered at the *M*(3) site, with the *Ca* site filled mainly with Ca, traces of Sr, and perhaps minor Mn^{2+}, and the *Na* site occupied dominantly by Na. Deficiency of Na is a result of the substitution $\square + {}^{M(2)}Fe^{3+} \rightarrow Na + {}^{M(2)}Fe^{2+}$.

In the classification of Strunz (Strunz and Nickel, 2001), maneckiite belongs to class 08.CF Phosphates, Arsenates, Vanadates with large and medium-sized cations, $RO_4:H_2O > 1:1$; (08.CF.05). In the classification of Dana (Gaines *et al.*, 1997), it belongs to class 40.02 Hydrated Phosphates, etc.; 40.02.10 Wicksite group; member 40.02.10.04. Maneckiite partly corresponds to UM1985-09-PO: CaFeHMn mineral defined as $(Mn,Fe^{3+},Fe^{2+},Mg,Ca,Na)_7Ca_2(PO_4)_6$ (Peacor *et al.*, 1985), suggested as "likely the Mn-analogue of wicksite" (Smith and Nickel, 2007; http://pubsites.uws.edu.au/ima-cnmnc/).

Origin

At Michałkowa, maneckiite occurs in an anatectic lithium-caesium-tantalum (LCT) pegmatite, coeval with the younger stage of Góry Sowie Block metamorphism at 380–370 Ma [370 ± 4 Ma,

TABLE 6. Refined site-scattering values and assigned site-populations in maneckiite.

Site	Refined site-scattering (epfu)	Assigned site-population (apfu)	<bond length> (Å)	Coordination number	Sum of ionic radii (Å)*
M(1)	42.31(9)	0.69 Mg + 1.31 Fe^{2+}	2.134	[6]	2.126
M(2)	41.04(9)	0.78 Mg + 1.22 Fe^{3+}	2.046	[6]	2.041
M(3)	23.5(7)		2.200	[6]	–
M(3A)	22.5(6)	1.92 Mn + 0.08 Mg	2.171	[5]	–
M(3B)	3.0(2)		2.112	[4]	–
Ca	40.18(9)	2.00 Ca	2.521	[8]	2.493
Na	9.93(7)	0.90 Na	2.468	[6]	2.560

*Ionic radii according to Shannon (1976).

https://doi.org/10.1180/minmag.2016.080.127 Published online by Cambridge University Press

TABLE 7. Simulated powder pattern for maneckiite.

I	*d* (Å)	*h*	*k*	*l*	*I*	*d* (Å)	*h*	*k*	*l*	*I*	*d* (Å)	*h*	*k*	*l*
17	6.458	0	2	0	30	2.121	4	3	3	10	1.666	2	5	5
16	6.263	2	0	0		–	1	6	0		–	0	4	6
13	5.832	0	0	2		–	1	5	3	12	1.652	7	2	2
14	4.496	2	2	0	12	2.088	3	3	4		–	4	0	6
9	4.328	0	2	2		–	6	0	0	17	1.638	4	1	6
5	4.195	2	2	1	12	2.045	2	4	4	13	1.634	5	6	0
7	4.053	2	1	2	10	1.965	6	0	2		–	5	5	3
10	3.562	2	2	2	9	1.913	3	6	0	10	1.609	7	1	3
22	3.520	3	2	0		–	3	5	3		–	2	4	6
68	**3.020**	**4**	**0**	**1**	6	1.900	1	1	6		–	6	5	1
	–	1	4	1	9	1.854	6	3	1	7	1.599	3	6	4
29	2.942	4	1	1		–	3	3	5		–	3	5	5
	–	2	2	3		–	6	0	3		–	6	4	3
78	**2.916**	**0**	**0**	**4**		–	2	1	6	8	1.572	4	7	1
31	**2.869**	**2**	**4**	**0**	6	1.823	5	2	4		–	5	6	2
35	**2.844**	**0**	**1**	**4**	8	1.780	4	4	4		–	1	6	5
30	**2.825**	**0**	**4**	**2**		–	5	5	1	11	1.556	0	8	2
100	**2.759**	**4**	**0**	**2**	14	1.753	4	6	1			0	5	6
20	2.698	4	1	2		–	6	4	0					
23	2.575	2	4	2	15	1.723	7	2	0					
19	2.495	3	4	1		–	3	4	5					
12	2.472	1	5	1	11	1.716	3	6	3					
13	2.437	1	4	3		–	4	3	5					
12	2.336	2	5	1		–	1	6	4					
	–	5	2	0			1	5	5					
9	2.323	4	3	2	8	1.705	2	3	6					
7	2.258	2	1	5		–	3	2	6					
8	2.156	3	5	1	6	1.693	4	6	2					
	–	2	1	5		–	5	1	5					
	–	0	6	0		–	6	3	3					

The strongest lines are given in bold.

Lutomia muscovite Ar-Ar dating, van Breemen *et al.* (1988); 383–370 Ma, Zagórze Śląskie zircon SHRIMP dating, Timmermann *et al.* (2000); 377.6 ± 1.3 Ma, Piława Górna monazite-(Ce) SHRIMP dating and 380.7 ± 2.4 Ma and uraninite CHIME dating; Turniak *et al.* (2015)]. The mineral seems to be a product of Na- and Ca-metasomatism induced by a high-temerature fluid released, under cooling, from a hydrosaline melt coexisting with an aluminosilicate melt, both formed by dissolution of a parental P-bearing silicate melt [see Simmons and Webber (2008) and discussion therein]. Maneckiite represents an early metasomatic phase crystallized in the outer zone of phosphate nodules close to the border with aluminosilicate melt, which could be the source of Al^{3+} found in some maneckiite crystals as well as grains of phosphates of the arrojadite group or lazulite. The crystals of Al-bearing maneckiite, with a Mn/(Mn+Fe) ratio ranging generally from 0.25 to 0.35, suggest an earlier crystallization in relation to typical Al-free maneckiite, showing higher values of the ratio, generally above 0.40. As with tassieite, another member of the wicksite group (Grew *et al.* 2007), maneckiite is associated closely with fluorapatite.

Acknowledgements

Ther authors thank members of the IMA CNMNC, Fernando Colombo, Peter Leverett and an anonymous reviewer for their comments on this manuscript, and Mark Cooper with his help with the crystallographic aspects of this work. The studies were supported by a National Science Centre Poland grant 2015/17/N/ST10/02666 to AW, an AGH UST grant 11.11.140.319 to AP, and by a Canada Research Chair in

https://doi.org/10.1180/minmag.2016.080.127 Published online by Cambridge University Press

Crystallography and Mineralogy to FCH and by a Natural Sciences and Engineering Research Council of Canada Discovery grant, and by Canada Foundation for Innovation grants to FCH.

References

Bartelmehs, K.L., Bloss, F.D., Downs, R.T. and Birch, J. B. (1992) EXCALIBR II. *Zeitschrift für Kristallographie*, **199**, 185–196.

Bianchi, R, Pilati, T. and Mannussi, G. (1987) Crystal structure of grischunite. *American Mineralogist*, **72**, 1225–1229.

Aftalion, M. and Bowes, D.R. (2002) U–Pb zircon isotopic evidence for Mid–Devonian migmatite formation in the Gory Sowie domain of the Bohemian Massif, Sudeten Mountains, SW Poland. *Neues Jahrbuch für Mineralogie, Monatshefte*, **4**, 182–192.

Bröcker, M., Żelaźniewicz, A. and Enders, M. (1998) Rb–Sr and U–Pb geochronology of migmatitic gneisses from the Góry Sowie (West Sudetes, Poland): the importance of Mid-Late Devonian metamorphism. *Journal of the Geological Society, London*, **155**, 1025–1036.

Brueckner, H.K., Blusztajn, J. and Bakun-Czubarow, N. (1996) Trace element and Sm–Nd "age" zoning in garnets from peridotites of the Caledonian and Variscan mountains and tectonic implications. *Journal of Metamorphic Geology*, **14**, 61–73.

Cámara, F., Oberti, R., Chopin, C. and Medenbach, O. (2006) The arrojadite enigma: I. A new formula and a new model for the arrojadite structure. *American Mineralogist*, **91**, 1249–1259.

Černý, P. and Ercit, T.S. (2005) The classification of granitic pegmatites revisited. *The Canadian Mineralogist*, **43**, 2005–2026.

Cooper, M.A. and Hawthorne, F.C. (1997) The crystal structure of wicksite. *The Canadian Mineralogist*, **35**, 777–784.

Gaines, R.V., Skinner, H.C., Foord, E.E., Mason, B. and Rosenzweig, A. (1997) *Dana's New Mineralogy.* 8th Edition. John Wiley & Sons, New York, USA.

Galliski, M.A., Cooper, M.A., Hawthorne, F.C. and Černý, P. (1999) Bederite, a new pegmatite phosphate mineral from Nevados de Palermo, Argentina: Description and crystal structure. *American Mineralogist*, **84**, 1674–1679.

Gordon, S.M., Schneider, D.A., Manecki, M. and Holm, D.K. (2005) Exhumation and metamorphism of an ultrahigh-grade terrane: geochronometric investigations of the Sudetes Mountains (Bohemia), Poland and Czech Republic. *Journal of the Geological Society, London*, **162**, 841–855.

Graeser, S., Schwander, H. and Suhner, B. (1984) Grischunite, ($CaMn_2[AsO_4]_2$), a new mineral species from the Swiss Alps. *Schweizerische Mineralogische und Petrographische Mitteilungen*, **64**, 1–10 [in German with English abstract].

Grew, E.S., Armbruster, T., Medenbach, O., Yates, M.G. and Carson, Ch.J. (2007) Tassieite, $(Na,\square)Ca_2(Mg,Fe^{2+},Fe^{3+})_2(Fe^{3+},Mg)_2(Fe^{2+},Mg)_2(PO_4)_6\cdot 2H_2O$, a new hydrothermal wicksite-group mineral in fluorapatite nodules from granulite-facies paragneiss in the Larsemann Hills, Prydz Bay, East Antarctica. *The Canadian Mineralogist*, **45**, 293–305.

Hawthorne, F.C, Ungaretti, L. and Oberti, R. (1995) Site populations in minerals: terminology and presentation of results of crystal-structure refinement. *The Canadian Mineralogist*, **33**, 907–911.

Jabłońska, J. (2015) *Mineralogical characteristics of feldspars from pegmatites near Michałkowa in the Sowie Mountains*. MSc thesis, Faculty of Earth Sciences and Environmental Management, University of Wrocław, Wrocław [in Polish with English abstract].

Kampf, A.R., Mills, S.J., Housley, R.M., Favreau, G., Boulliard, J-C. and Bourgoin, V. (2012) Angarfite, $NaFe_5^{3+}(PO_4)_4(OH)_4\cdot 4H_2O$, a new mineral species from the Angarf-Sud pegmatite, Morocco: description and crystal structure. *The Canadian Mineralogist*, **50**, 781–791.

Kryza, R. (1981) Migmatization in gneisses of the northern part of the Sowie Góry, Sudetes. *Geologia Sudetica,* **16**, 7–91 [in Polish, English summary].

Kryza, R. and Fanning, C.M. (2007) Devonian deep-crustal metamorphism and exhumation in the Variscan Orogen: evidence from SHRIMP zircon ages from the HT–HP granulites and migmatites of the Góry Sowie (Polish Sudetes). *Geodinamica Acta*, **20**, 159–176.

Łodziński, M. (2007) Mineralogical study of beryls from Polish and Czech Sudetes. *Prace Mineralogiczne, PAN Kraków*, **93**, 5–179 [in Polish, English summary].

Łodziński, M. and Sitarz, M. (2009) Chemical and spectroscopic characterization of some phosphate accessory minerals from pegmatites of the Sowie Góry Mts, SW Poland. *Journal of Molecular Structure*, **924–926**, 442–447.

Mandarino, J.A. (1981) The Gladstone – Dale relationship: Part IV. The compatibility concept and its application. *The Canadian Mineralogist*, **19**, 441–450.

Mazur, S., Aleksandrowski, P., Kryza, R. and Oberc-Dziedzic, T. (2006) The Variscan Orogen in Poland. *Geological Quarterly*, **50**, 89–118.

Novák, M. (2005) Granitic pegmatites of the Bohemian Massif (Czech Republic); mineralogical, geochemical and regional classification and geological significance. *Acta Musei Moraviae - Scientiae Geologicae*, **90**, 3–75 [in Czech, English summary].

O'Brien, P.J., Kröner, A., Jaeckel, P., Hegner, E., Żelaźniewicz, A. and Kryza, R. (1997) Petrological

https://doi.org/10.1180/minmag.2016.080.127 Published online by Cambridge University Press

and isotope studies on Palaeozoic high-pressure granulites. Góry Sowie Mts, Polish Sudetes. *Journal of Petrology*, **38**, 433–456.

Peacor, D.R., Dunn, P.J., Ramik, R.A., Campbell, T.J. and Roberts, W.L. (1985) A wicksite-like mineral from the Bull Moose Mine, South Dakota. *The Canadian Mineralogist*, **23**, 247–249.

Pieczka, A., Hawthorne, F.C., Gołębiowska, B. and Włodek, A. (2015*a*) Maneckiite, IMA 2015-056. CNMNC Newsletter No. 27, October 2015, page 1227; *Mineralogical Magazine*, **79**, 1229–1236.

Pieczka, A., Szuszkiewicz, A., Szełęg, E., Janeczek, J., Nejbert, K. (2015*b*) Granitic pegmatites of the Polish part of the Sudetes (NE Bohemian massif, SW Poland). *7th International Symposium on Granitic pegmatites*, *Książ, Poland, June 17–19, 2015*. *Fieldtrip Guidebook C*, 73–103.

Pouchou, J.L. and Pichoir, F. (1985) "PAP" procedure for improved quantitative microanalysis. Pp. 104–106 in: *Microbeam Analysis* (J.T. Armstrong, editor). San Francisco Press, San Francisco, California, USA.

Shannon, R.D. (1976) Revised effective ionic radii and systematic studies of interatomic distances in halides and chalcogenides. *Acta Crystallographica*, **A32**, 751–767.

Sheldrick, G.M. (2008) A short history of SHELX. *Acta Crystallographica*, **A64**, 112–122.

Sheldrick, G.M. (2015) Crystal structure refinement with *SHELXL*. *Acta Crystallographica Section C*, **71**, 3–8.

Simmons, W.B. and Webber, K. (2008) Pegmatite genesis: state of art. *European Journal of Mineralogy*, **20**, 421–438.

Smith, D.G.W. and Nickel, E.H. (2007) A system for codification for unnamed minerals: report of the Subcommittee for Unnamed Minerals of the IMA Commission on New Minerals, Nomenclature and Classification. *The Canadian Mineralogist*, **45**, 983–1055.

Strunz, H. and Nickel, E.H. (2001) *Strunz Mineralogical Tables*, Ninth Edition. Schweizerbart'sche Verlagsbuchhandlung, Stuttgart, Germany.

Sturman, B.D., Peacor, D.R. and Dunn, P.J. (1981) Wicksite, a new mineral from northeastern Yukon Territory. *The Canadian Mineralogist*, **19**, 377–380.

Szuszkiewicz, A., Szełęg, E., Pieczka, A., Ilnicki, S., Nejbert, K., Turniak, K., Banach, M., Łodziński, M., Różniak, R., Michałowski, P. (2013) The Julianna pegmatite vein system at the Piława Górna mine, Góry Sowie Block, SW Poland – preliminary data on geology and descriptive mineralogy. *Geological Quarterly*, **57**, 467–484.

Timmermann, H., Parrish, R.R., Noble, S.R. and Kryza, R. (2000) New U–Pb monazite and zircon data from the Sudetes Mountains in SW Poland; evidence for a single-cycle Variscan Orogeny. *Journal of the Geological Society, London*, **157**, 265–268.

Turniak, K., Pieczka, A., Kennedy, A.K., Szełęg, E., Ilnicki, S., Nejbert, K., Szuszkiewicz, A., (2015) Crystallisation age of the Julianna pegmatite system (Góry Sowie Block, NE margin of the Bohemian massif): evidence from U-Th-Pb SHRIMP monazite and CHIME uraninite studies. *7th International Symposium on Granitic Pegmatites, PEG 2015 Książ, Poland. Book of Abstracts*, 111–112.

van Breemen, O., Bowes, D.R., Aftalion, M. and Żelaźniewicz, A. (1988) Devonian tectonothermal activity in the Sowie Góry gneissic block, Sudetes, southwestern Poland: evidence from Rb–Sr and U–Pb isotopic studies. *Annales Societatis Geologorum Poloniae*, **58**, 3–10.

Websky, M. (1868) Über Sarkopsid und Kochelite, zwei neue Minerale aus Schlesien. *Zeitschrift der Deutschen Geologischen Gesellschaft*, **20**, 245–257.

Żelaźniewicz, A. (1990) Deformation and metamorphism in the Góry Sowie gneiss complex, Sudetes, SW Poland. *Neues Jahrbuch für Geologie und Paläontologie, Abhandlungen*, **179**, 129–157.

https://doi.org/10.1180/minmag.2016.080.127 Published online by Cambridge University Press